Electron Transport in Lead Selenide Nanocrystal Arrays

by

Maria C Schriver

Submitted to the Department of Physics
in partial fulfillment of the requirements for the degree of

Bachelor of Science in Physics

at the

MASSACHUSETTS INSTITUTE OF TECHNOLOGY

June 2005

Author .....
Department of Physics
May 6,2005

Certified by .....
Marc Kastner
Donner Professor of Physics and Department Head
Thesis Supervisor

Accepted by .....
David E. Pritchard
Thesis Coordinator

Electron Transport in Lead Selenide Nanocrystal Arrays

by

Maria C Schriver

Submitted to the Department of Physics
on May 6,2005, in partial fulfillment of the
requirements for the degree of
Bachelor of Science in Physics

Abstract

I have investigated electrical properties of arrays of lead selenide (PbSe) nanocrystals (NC's) of approximately $6nm$ diameter. The films become substantially more conducting when annealed at 400K, although no chemical changes of the capping layer occur at this low temperature. There is no evidence based on TEM images of annealed and unannealed films that the interparticle spacing changes at 400K. The dependence of the conductance on the voltage applied to a gate separated from the sample by $350nm$ of SiO_2 was also measured. At 77K and 150K, a U-shaped curve is observed with a minimum in conductance near zero gate voltage, indicating that both electrons and holes are injected. At 294K, the conductance falls monotonically with increasing gate voltage, indicating injection of holes only. I calculate the electron and hole mobilities, μ_e and μ_h at 77K and 150K and find effective mobilities 10 orders of magnitude smaller than those of bulk PbSe at 77K.

Thesis Supervisor: Marc Kastner
Title: Donner Professor of Physics and Department Head

Acknowledgments

I want to thank Marc Kastner for unfailing encouragement and a constant sense of excitement about physics and about this experiment. His amazing ability to explain an intricate physical concept with a seemingly simple illustration has been extremely helpful as I've studied this new field. I have gained a tremendous amount of understanding from him, both about the specific physics I've studied and about how to think about physics in general. Marc's skill as a teacher and mentor has stemmed from an ability to make me feel excited about the work I was doing and at the same time to make me realize how much I had to learn before I could really understand that work.

I thank Tamar Mentzel for working with me on this project over the past 9 months. She is one of the most patient people I have ever worked with and provided excellent balance for my less patient personality. Thanks also to our collaborators in Moungi Bawendi's research group, especially to Venda Porter for preparing films, taking TEM images, and for patiently answering all of Tamar's and my questions about chemistry. Thanks to the other graduate students and post-docs in the Kastner lab for being great people to work with, especially Sami Amasha who was always willing to give up his time to help me when I had a problem with a measurement.

Finally, I thank my parents for supporting all of my educational decisions without ever making me feel pressured. Their faith in my ability to make good decisions and learn from bad ones has been invaluable during my time at MIT.

Contents

List of Figures

List of Tables

Chapter 1

Introduction

Quantum dots are academically fascinating because they are a realization of the most basic problem of quantum mechanics, the particle in a box. Electrons are physically confined to nanometer-sized crystals, the physical dimensions of which determine allowed energy levels. This confinement results in unique electrical and optical properties which in turn give rise to a wide range of potential applications.

1.1 General Background

A quantum dot can be thought of as a potential well in which the number of electrons is well defined. This is accomplished by making oases of metal or semiconductor material which are small enough that the energy required to add a single electron is larger than the thermal energy scale (k_BT). The energy required to add a single electron is at least $E_c = \frac{e^2}{2C_d}$ where C_d is the capacitance between the dot and its surroundings. As the physical dimensions of the dot decrease, C_d falls and the energy required to add an electron increases. At size scales of 100's of nanometers and smaller, E_c can become larger than k_BT and the number of electrons on the dot becomes well-defined.

A quantum dot with physical dimensions on the order of or smaller than the Bohr radius of the electrons in contains, can be thought of as a spherical potential well which confines its

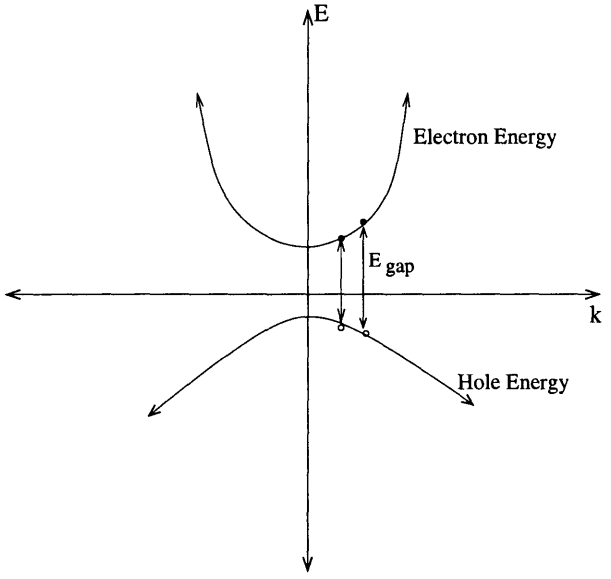

Figure 1-1: **Quantum dot energy diagram** Energy is a quadratic function of k. The dots represent k_{min} for two different sized quantum dots. The smaller k_{min} corresponds to a larger diameter quantum dot. The lower curve is the energy of a hole as a function of k and the upper curve is the energy of an electron. The gap between the two curves represents the energy necessary to create an electron-hole pair in the dot. Obviously, the necessary energy increases as size decreases. This diagram is very simplistic and for conceptual purposes only. It ignores the finite energy of the quantum dot walls, the potential inside the dot and the interaction between the electron and hole.

electrons. Thus, an electronic wavefunction must be zero at all edges of the sphere, which requires the wavelength, λ, of the wavefunction to be sufficiently small. A minimum value for λ translates into a maximum value for $k = 2\pi/\lambda$ and a maximum value for δE, the energy of an electron-hole pair, as seen in Figure 1-1 [1].

The optical results of these size-controlled energy levels are impressive. The absorbance energy of quantum dots rises as their size decreases. Additionally, quantum dots made from several semiconductor materials are fluorescent. Just as the absorbance depends on the dots size, so does the main fluorescence wavelength. Size-tunable fluorescence is not only visually exciting when the main band gap is tunable within the visible range, as it is for CdSe, it also has potentially wide application to various endeavors requiring fluorescent markers [8] [6].

In a sufficiently small dot, the band gap can be on the order of E_c. In this case, the

energy levels have a discrete effect on the energy required to add an electron to the dot, and that energy becomes $E_d = E_c + \delta E$, where δE is the spacing between energy levels. Because of the well-defined electron occupation and discrete energy levels, quantum dots share many characteristics with atoms and are often referred to as artificial atoms.

Extending the artifical atom analogy, 2- and 3-dimensional arrays of quantum dots can be thought of as artificial solids. Of course, the unique size of the NC's and the physical confinement of electrons to individual "atoms" endow these artificial solids with electrical and optical properties which are very different from conventional solids. In this thesis, I report the investigation of electrical properties in artificial solids consisting of arrays of lead selenide (PbSe) nanocrystals (NC's). These are individual spherical crystals of PbSe grown to about 6nm in diameter and separated by a layer of oleic acid, which provides a potential barrier between neighboring crystals.

1.2 Previous Work

A large body of research exists describing electrical and optical properties of cadmium selenide (CdSe) nanocrystals. Unfortunately, the large bandgap in CdSe leads to very low carrier concentrations and thus low conductivities, making measurements of stable dark currents impossible [1]. All measurements of dark current have been of current transients as charge flows into the film. These transients do appear to respond to charge injection, which is promising. Conduction dependence on charge injection indicates that electrons can be injected into the CdSe films, but not necessarily holes [2]. Leatherdale et al. [3] have been successful in measuring and characterizing photoconductivity in CdSe, including investigations of size, electric field, and temperature dependence of photoconductivity.

While CdSe has been an interesting material to study, the very low dark conductivity is very limiting. PbSe films solve this problem because dark conductivity is much higher and can be measured reliably. PbSe also has a substantially smaller band gap than CdSe (0.28eV in bulk [5]). This increases the potential experimental value of PbSe because the

energy levels on either side of the gap may be closer to those of metal electrodes used to inject charge, making charge injection easier. It also lowers δE, lowering the energy cost of charge injection.

PbSe is also a more promising material than CdSe because the Bohr radii of the electron and hole are both $23nm$ [4], so it is possible to confine both electrons and holes in a nanocrystal a few nm across. In contrast, while the electron and exciton Bohr radii in CdSe are on the order of $\sim 10nm$, the hole Bohr radius is only on the order of $\sim 1nm$, making effective confinement of holes very difficult in CdSe nanocrystals.

However, for a long time, a good method for preparation of PbSe nanocrystals was not known. Murray et al [8] published a method in 2001 which allowed for the preparation and deposition of highly monodisperse (or consistently sized) PbSe nanocrystals. The NC's can be deposited as films onto fabricated devices, allowing various measurements of their properties. This process has allowed some research to be done on PbSe NC's, including characterization of their absorbance properties [9] and injection of both holes and electrons in an electrochemical cell [5].

Additional work on PbSe NC's includes various methods for preparing the NC's and preparation of PbTe and PbS NC's as well as preparation of lead chalcogenide NC's in various shapes such as rods, cubes, wires, and multipods, which are shaped triangularly or tetrahedrally with rods extending from a central point [7] [10]. These different shapes offer the possibility of improved conductivity or different conductivities along different lattice dimensions.

1.3 Applications

Because NC's of a given semiconductor have a larger bandgap than the bulk material, they have high fluorescence efficiency. Thus, they can be used as fluorescent markers in biological applications [7]. The band gap of bulk PbSe is at 0.278eV [5], which is in the IR. This means that PbSe nanocrystals of various nm-scale sizes will have band gaps covering the

near-IR part of the spectrum, which is important for fluorescence materials [6] and biological imaging because there are currently few materials that are good fluorophores in the IR [7]. The conductivity of the films is greatly enhanced when they are illuminated with light of sufficiently high energy, giving NC's the potential to be used in photodetectors [3].

Current flow through semiconductor NC's can potentially be carefully tuned by electrostatically varying concentrations of charge carriers. This ability could lead to applications in building transistors a smaller scale than traditional silicon transistors. Because of the relatively high currents in traditional transistors, power dissipation becomes extremely high as the number of transistors packed onto a single chip increases. Transistors made from semiconductor NC's have lower currents and the conduction occurs through quantum tunneling rather than classical conduction mechanisms, reducing the power demand and thus the energy lost and heat created.

The strong confinement of electrons in semiconductor NC's holds promise for novel computing applications. Quantum computing applications involving manipulation of the wavefunction of an electron confined to a quantum dot have been proposed [11]. Because of the capacitive interactions between neighboring NC's in an array, it is thought that this system may yield interesting collective computing properties. Systems with individual computational elements (bits or qubits in quantum computing) which interact with one another provide an opportunity to model the kind of computation that occurs in the human brain, in which neurons interact strongly with each other. This kind of system is known as a neural network and due to the short and long range electrostatic linking between semiconductor NC's, they may potentially be a good system in which to implement neural networking [12] [11].

1.4 Thesis Outline

In this thesis, I will first describe some of the theory behind charge injection and conductivity enhancement in nanocrystal films. In Chapter 3, I will describe the experiment we use to

measure this injection, and then present results of the effect of annealing on conductivity in Chapter 4 and the effect of capacitive charge injection on conductivity in Chapter 5.

Chapter 2

Theory

2.1 Electronic Wavefunctions in NC's

If we model an NC as a perfect sphere of radius a with potential

$$V(r) = 0 \qquad r < a \tag{2.1}$$

$$V(r) = \infty \qquad r > a \tag{2.2}$$

we can solve the Schrodinger equation to yield a wavefunction of the form

$$\psi(r, \theta, \phi) = A_{nl} j_l(\beta_{nl}, \frac{r}{a}) Y_l^m(\theta, \phi) \tag{2.3}$$

where $A_{n,l}$ is a normalization factor, j_l is the l^{th} spherical Bessel function and $\beta_{n,l}$ is the n^{th} zero of j_l. Y_l^m is the spherical harmonic corresponding to l and m. This model is a little bit too simplistic in that the potential inside the well is actually the periodic potential of the semiconductor crystal. According to Bloch's theorem for periodic potentials, the

wavefunction should have the form

$$\psi(\vec{r}) = u_k(\vec{r})e^{\vec{k}\cdot\vec{r})} \tag{2.4}$$

We can replace the plane wave in equation 2.4 with the wavefunction in equation 2.3, giving the energy of an electron in a given band as

$$E_{nl} = \frac{\hbar^2}{2m_e a^2}\beta_{nl}^2 \tag{2.5}$$

These are the discrete energy levels that make the term "artificial atom" so fitting. The energy required to add an electron to the film is $E_{nl} + E_c$ where E_c is the capacitive charging energy. The energy of a corresponding hole is $E_{nl} * \frac{m_e}{m_h} + E_v$. The energy required to create an electron-hole pair is $E_{nl}(1 + \frac{m_e}{m_h}) + E_c + E_v - E_{coul}$ where E_v is the valence energy which corresponds to E_c and E_{coul} is the coulomb interaction energy between the two charged particles.

2.2 Conduction through NC films

Some of the most useful applications of semiconductor nanocrystals, including computer memory and quantum computing applications, will stem from an ability to control current levels through NC films. This can be accomplished by applying a steady voltage between source and drain electrodes and controlling the conductivity of the film between the two electrodes.

The conductivity through nonmetallic solids can be described by:

$$\sigma = ne\mu_e + pe\mu_h \tag{2.6}$$

Where n and p are the concentrations of electrons and holes, respectively, and μ_e and μ_h are the respective mobilities. e is the elementary charge. Thus, conductivity should increase

linearly with carrier concentration, with the slope depending on the mobility of the carrier.

Conduction through the film occurs by quantum tunneling, since the organic layer separating adjacent dots presents a high energy barrier for charge carriers. However, hopping does not necessarily occur between nearest neighbors. Electrons will prefer to hop to sites with a combination of the lowest activation energy, δE, and the shortest distance [13]. δE is a measure of the potential difference between the two sites and falls off as distance increases.

Conduction through the films is not ohmic. Middleton and Wingreen predict that at temperatures low enough that $k_B T < e^2/C$, where C is the capacitance between an individual NC and a metal gate which is separated from the film by a dielectric, I-V curves will behave as a power law [14],

$$I \sim (V/V_T - 1)^{\xi} \tag{2.7}$$

where V_T is some threshold voltage below which current does not flow because the disorder of the film creates a random potential gradient which overcomes the applied voltage at individual NC sites [15]. For NC's of diamater 6nm, this capacitive energy is $\sim 10meV$, which is lower than $k_B T$ for all T's below 100K. In this low temperature regime, current flows only through a few low energy paths. The innate disorder of the films creates a variance in energy cost for different possible paths across the film, depending on which NC's electrons hop through in the process and the potential differences between those NC's. As voltage is increased, both the conduction across the paths in use and the number of available paths increase. Using equation 2.7, Middleton and Wingreen predict $\xi = 5/3$ for an infinite 2-dimenstional array of NC's.

2.3 Tuning the Conduction

According to equation 2.6, we can improve the conductivity of a film by increasing the concentration of charge carriers. One way to do this that has been successful in CdSe films is to irradiate the film with light of a higher energy than the band gap of the NC's. This

significantly improves the conductivity and the current measured in this way is referred to as photocurrent, as opposed to dark current [3]. This works because each photon creates an exciton, a free hole and electron, freeing two charge carriers. The overall charge of the film does not change-for every free electron created, a free hole is also created. Photoconductivity is dependent on both the size of the NC and on the temperature. In order for the two carriers to conduct current, they must be separated into two different NC's. This is easier if they are confined to a bigger diameter NC, because the two charges are allowed to separate from each other more within the NC, reducing the Coulomb attraction and allowing one to leave the NC with a lower energy cost. Additionally, the probability of charge separation happening before the hole and electron recombine depends on a nonradiative recombination rate k_{nr} and a radiative recombination rate k_r. k_{nr} increases with increasing temperature, so charge separation efficiency falls and consequently photoconductivity falls with increasing temperature [1].

An alternative way to increase the number of charge carriers is to add free charge, changing the overall charge of the film. Guyot-Sionnest et al. have been successful in injecting electrons into CdSe films [16] and both electrons and holes into PbSe films [5]. This is done in an electrochemical cell where a salt solution, such as $LiClO_4$ in acetonitrile, carries charge from an electrode to the film. They observe charge injection both through increased conductivity and through a bleach of the main absorbtion peak of the NC's as the conduction band filled with electrons, leaving a lower probability for electrons in the valence band to transition into the conduction band by absorbing a high energy photon.

In this experiment, we will add free charge capacitively rather than chemically. The NC film will essentially form one plate of a parallel-plate capacitor with a metal gate forming the other plate. Between the two plates is a dielectric material, SiO_2 in our case. When a voltage is applied to the metal gate, charge collects on both plates of the capacitor according to

$$Q = V_g * \frac{A * \epsilon}{d} \tag{2.8}$$

where Q is the total charge, A is the area of the plates, ϵ is the dielectric constant of the material between the plates and d is the distance between the plates. Because we are concerned with charge concentration, Q/A, we will prefer to look at

$$\frac{Q}{A} = V_g * \frac{\epsilon}{d} \tag{2.9}$$

Equation 2.6 implies that increasing carrier concentration always increases conductivitiy. While this is generally true for semiconductor NC films, because conduction in these films is different and more complicated than conduction in bulk semiconductors, this equation does not fully describe the dependence of conductivity on carrier concentration. Levitov predicts that at low temperatures, charge concentrations which correspond to 1/3 and 1/2 of a charge per NC will be especially stable and lead to minima in conductivity. Essentially, if there is 1 carrier for every 3 NC's in the hexagonal close-packed (hcp) lattice, the charges can assume a uniform configuration on lattice sites (NC's) which has minimal energy. Since the configuration is uniform, any movement of a single carrier upsets the configuration and thus raises the energy. If there are a few extra charges, they are defects in the uniform configuration. If the extra carriers move, the energy of the configuration is unchanged because the defect has simply moved to a new, but not unique, position. Thus, deviations from 1/3 and 1/2 filling fractions allow conduction [17]. Observation of this result may require long range hcp ordering of the film, which is difficult to achieve with current preparation techniques.

Chapter 3

Experimental Design

3.1 Structure of NC Films

NC films consist of lattices of nanometer sized semiconductor crystals. In order to passivate the surface of the crystals and to prevent the crystals from aggregating or bonding to one another, an organic capping layer is used between individual NC's. The capping molecule bonds to the NC surface, limiting any reactivity of the surface. Since the capping molecules bond to multiple NC's, they can also facilitate assembly. Capping layers are selected first for empirical success in preparing monodisperse, self assembled NC's of a particular material and preventing aggregation and precipitation during preparation. Cap exchanges may be done after the NC's have been deposited to replace the capping layer chosen for this reason with one that serves other purposes. A capping layer that presents a lower barrier to conduction may be chosen, or one that is shorter and will allow the NC's to pack closer together. A cartoon representation of an NC with a capping layer is shown in Figure 3-1.

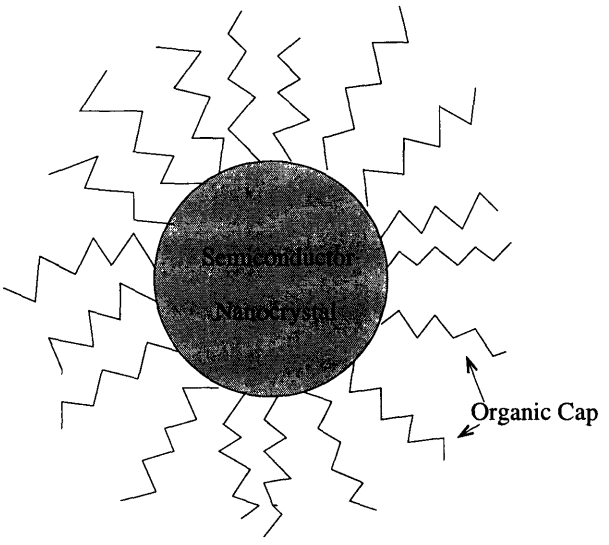

Figure 3-1: **Cartoon of NC with capping molecules bonded to it.**

3.2 Making the Dots

The PbSe NC films studied in this thesis have a main absorption band at $0.73eV$. This corresponds to a diameter of approximately $6nm \pm 10\%$ [9]. The capping layer is oleic acid, which provides about $0.5 - 1nm$ spacing between adjacent NC's.

To prepare the NC's, 0.6ml oleic acid and 0.382g lead acetate are dissolved in 21ml of diphenyl ether. The flask is flushed of oxygen by alternately degassing it and filling it with Argon gas four times. The solution is then heated to 155°C under argon gas to fully dissolve the lead acetate. It is then cooled to 70°C and degassed. After two hours, it is reheated to 155°C and 5ml of 1.0M TopSe is injected. The injection cools the solution. PbSe nucleates at 155°C, so nucleation is limited by the cooling time. After nucleation, the solution is heated again until it reaches 155° (about 3.5 minutes), during which time the NC's continue to grow, but no longer nucleate. This produces monodisperse crystals of cubically structured PbSe.

The NC's are separated from their growth solution by adding methanol to the solution, which causes the dots to precipitate with the oleic acid capping layer. The solution is then centrifuged and the precipitate is redissolved in trichloro-trifluoro-ethane and forced

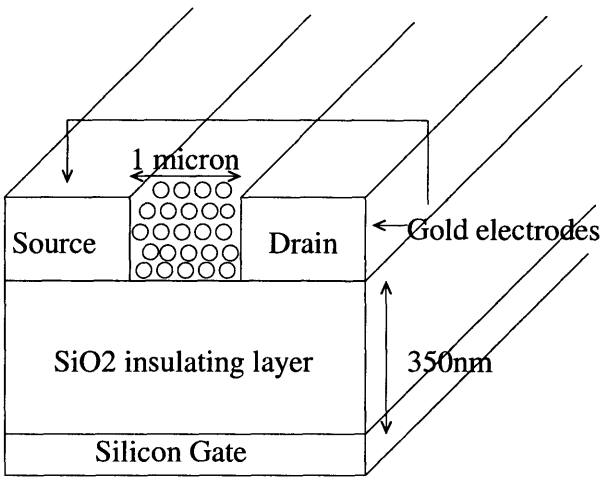

Figure 3-2: **Schematic of device used for measurement**

through a $0.2\mu m$ filter. This separation process is repeated once again. The second time, the precipitate is dissolved in a 9:1 mixture of hectane and octane and forced through a $0.1\mu m$ filter.

Finally, the dots are deposited by dropping one drop of solution onto a substrate and allowing it to dry overnight. The final film is about 50 layers, or $300nm$ thick.

This process produces spherical dots that self assemble into hexagonally-close packed (hcp) regions. However, this process does not produce long-range order in the film. It is possible to induce semiconductor NC's to self assemble into a long-range ordered hcp structure [1], but this was not done for this experiment.

3.3 Electrical Experiment

For this experiment, the NC's were deposited on a device consisting of a silicon gate with 350nm of SiO_2 grown on it. Gold source and drain electrodes were lithographically patterned on top of the SiO_2 before NC deposition. See Figure 3-2 for a schematic of our device.

We measure the conductance through the dots by applying a small bias, V_{sd}, at the source electrode and measuring the current at the drain electrode. Because the resisistivity of the

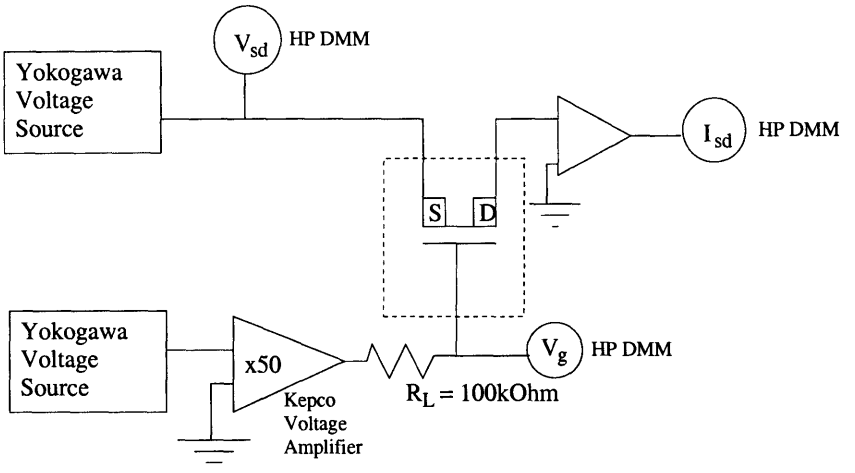

Figure 3-3: **Schematic of circuit**

film is very high ($10^9 - 10^{14}\Omega$), the current is amplified before being measured at an HP DMM. Charge is added to the film capacitively by applying a large voltage, V_g, to the Si gate. V_{sd} and V_g are monitored during the measurement. A schematic of our circuit is shown in figure (3-3).

Chapter 4

Effects of Annealing

Immediately after deposition, the NC films are extremely resistive. They are so resistive that it is not clear that currents through them are higher than the leakage current of the system. Measurements of devices before and after deposition show currents on the order of $\sim 100fA$ at $V_{sd} = 5V$. The fact that our leakage is of a similar magnitude as our current before annealing makes meaningful measurements before annealing difficult.

In order to conduct effective current measurements, we anneal the samples, which increases the conductivity, allowing measurable currents to pass. We have found that annealing for 24+ hours at 400K raises the conductance by 4 orders of magnitude. The conductance rises steadily for the entire annealing time and then flattens out after 24+ hours. If the process is stopped before the conductance stops rising, the conductance remains unstable when the sample is cooled to room temperature and measurement is impossible.

The increase in conductance is exponential in time, so it appears linear on a semi-log plot. Figure 4-1 shows the conductance at zero-bias as well as the current when $V_{sd} = 5V$. The graph covers a 27-hour period.

All zero-bias conductance data in this thesis were collected by analyzing $\Delta I/\Delta V_{sd}$ for intervals around $V_{sd} = 0V$ during sweeps from $V_{sd} = (-5V) - (+5V)$. Several small interval sizes were tried to confirm that the size of the interval did not change the values of $\Delta I/\Delta V_{sd}$,

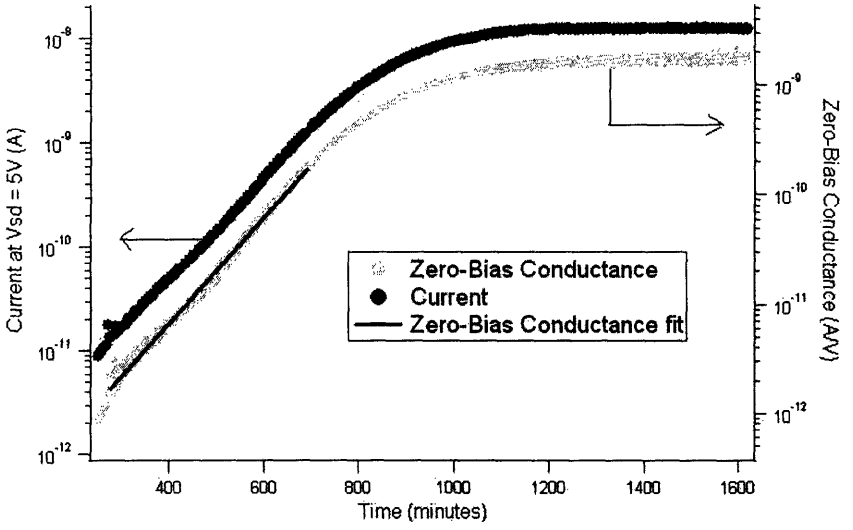

Figure 4-1: **Current at $V_{sd} = 5V$ and Zero-Bias conductance against time.** Current magnitude and zero-bias conductance against time at 400K. The data are well represented by an exponential curve.

indicating that the IV curve was linear in the area sampled.

The zero-bias conductance data is fit to an exponential curve with equation,

$$\sigma = Ae^{kt} \tag{4.1}$$

Where t is expressed in minutes. The fitted parameters are A = 7.69e-14 $\pm$ 1.73Ee-15 and k = 0.011 $\pm$ 4.47e-5 The reduced χ^2 for the fit is 1.21 assuming 10 % error on each point. This assumption is justified by the scatter of the points in the flat part at the end of the curve.

The explanation for the increase in conductivity is not clear. Other groups have observed CdSe NC's moving closer together after annealing at high temperatures [18]. This occurs as the organic capping layer changes chemically and the molecules become shorter, allowing the NC's to pack closer to one another. As the spacing between adjacent NC's falls, the tunneling probability should increase exponentially, which could explain the shape of the curve.

Table 4.1: **Average center-center spacings before and after annealing** TEM images are not all on the same scale.

Annealed for	Average spacing	σ
0 hours	6.36nm	0.392nm
12 hours	5.94nm	0.530nm
24 hours	6.30nm	0.450nm

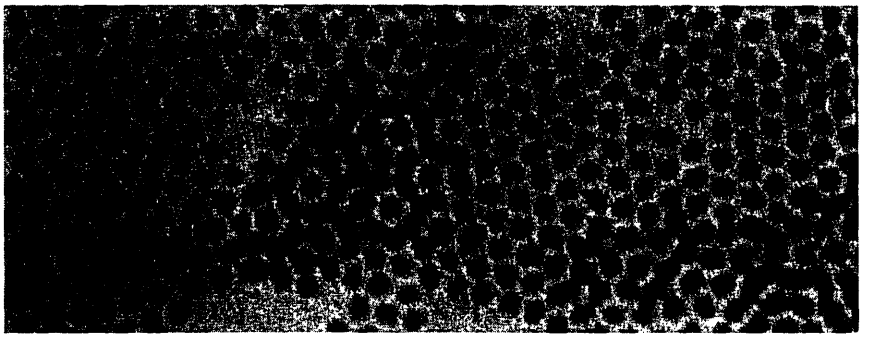

Figure 4-2: **TEM of film before annealing**

To determine whether this was happening, transmission electron microscope (TEM) images were taken of PbSe films before annealing, after 12 hours of annealing and afer 24 hours of annealing at 400K (Figures 4-2 to 4-4). The images were analyzed by selecting regions and taking a fourier transform of the image to determine the dominant frequency. It is assumed that the inverse of the most dominant frequency corresponds to the center to center spacing between NC's. This spacing includes the average diameter of the NC's added to the interparticle spacing created by the oleic acid. For each image, 5-10 regions were selected and analyzed. The frequencies were weighted by the strength of the fourier peak and averaged using those weights. The standard deviation (σ_f) of the set of frequencies was also calculated. The center to center spacing reported is the inverse of the weighted average of the frequencies and σ_s is calculated from σ_f. The average center to center spacings and standard deviations are shown in Table 4.1

These data do not support the conclusion that the NC's move closer together with time at 400K. Each average is within one standard deviation of the other averages, so it is impossible

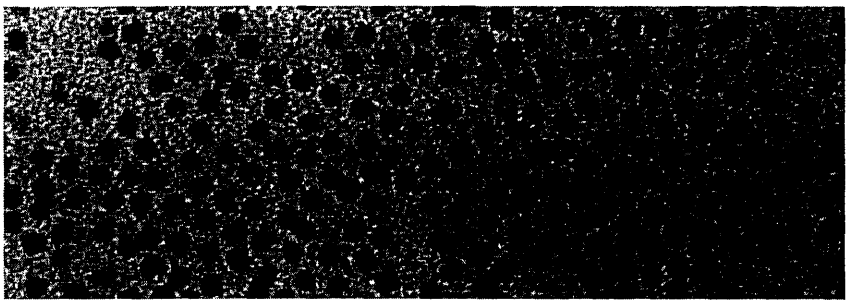

Figure 4-3: **TEM of film after annealing for 12 hours at 400K**

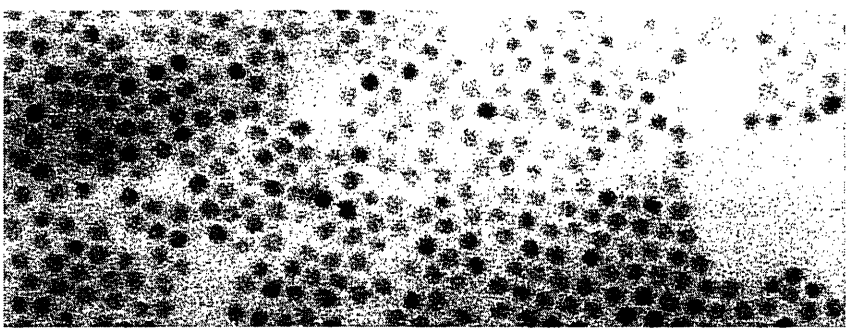

Figure 4-4: **TEM of film after annealing for 24 hours at 400K**

to conclude with any confidence that the interparticle spacing is changing at all. 400K is a very low temperature to see chemical changes, so this is not surprising. Oleic acid cross-links at around 410K, meaning that the double bond in the molecule breaks, allowing nearby molecules to bond to each other.

The TEM images, (Figures 4-2 to 4-4), seem to show very ordered NC arrays before annealing and less order afterwards. One hypothesis is that the higher temperature allows the NC's to move and some of them move closer together while others actually move farther apart, leaving the average spacing unchanged. In Middleton and Wingreen's model of conduction, this increase in disorder could itself improve conductance. If some of the NC's move closer together, it is possible that the lowest energy path across the gap becomes lower, while other paths become higher energy. However, the raising in energy of the high energy paths would not affect conductance, but the lowering in energy of the lowest energy path would, leading to the increase in conductance that we observe. This hypothesis is called into question by the fact that σ_s is lower after 24 hours than after 12. However, the sample annealed for 24 hours was a different sample with a higher concentration of NC's than the first two. Since this hypothesis relies on NC movements that would be unique to each sample, it is possible that a difference in concentration would lead to a difference in NC movements and to a difference in the variance of center to center spacing after annealing. Thus, while the data cannot be said to support this hypothesis, they also do not definitively refute it.

A more likely hypothesis is that heating boils off solvent that is left between the NC's after deposition. This could be a very slow process, as we observe. Removing solvent from the film could increase conductance in a few ways. The solvent, hexane, may present a substantially larger potential barrier to tunneling than the oleic acid alone does. Another possibility is that removal of solvent does, in fact, allow the NC's to move closer together. The films deposited for TEM measurements were of a low concentration and were monolayers, while the film on which the conductance measurement was done consisted of 50-100 layers of NC's. Hexane evaporates at room temperature and would have evaporated much more quickly from the monolayer than from our multi-layer film. Thus, it is possible that even before annealing,

the solvent had evaporated from the films used in the TEM measurement, resulting in no further evaporation during annealing and no change in interparticle spacing. The film we measured, on the other hand, would have held onto the solvent buried under several layers of NC's and released it only when heated, resulting in a reduction of interparticle spacing in that film. Finally, it is possible that the solvent creates localized states and traps charge carriers in them. When the solvent evaporates, it would release these charges and the carrier concentration in the film would increase, increasing conductivity.

Chapter 5

Gate Voltage Dependence

We measured IV curves at different gate voltages at room temperature both before and after annealing. Before annealing, we see no difference between IV curves taking with 0V on the gate and with 50V on the gate. There is an offset of $\sim 4pA$ which is due to current leaking from the gate through the SiO_2 layer to the drain electrode, but no difference in the conductance or in the slope of the IV curve (Figure 5-1). The conductance before annealing is on the same order of magnitude as the conductance measured before NC's are deposited, meaning that this V_g dependence measurement is not conclusive.

The IV curves after annealing show much larger currents. They also show a non-ohmic shape. The curves follow a power law of

$$I = 2.7 * 10^{-10} * V^{2.05} \tag{5.1}$$

Because we do not see a threshold voltage in the IV curves, we assume that V_T is much smaller than the voltages we are using and thus $V/V_T >> 1$, so we ignore the "1" in equation 2.7. The power of $\xi = 2.05 \pm 0.05$ is not too far from the power of 5/3 predicted by Middleton and Wingreen [14] for a 2-dimensional array. The difference may be accounted for by the fact that Middleton and Wingreen consider an infinite array, or by the larger

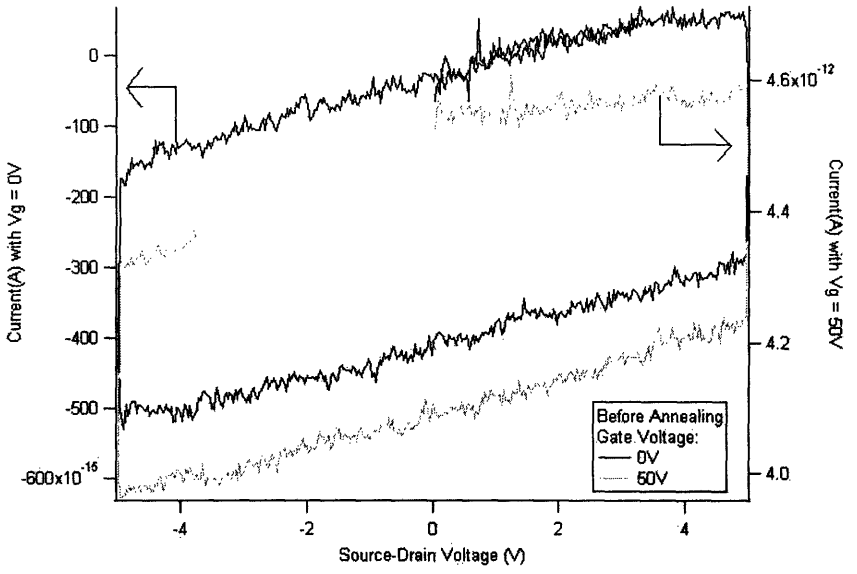

Figure 5-1: **IV curves before annealing.** The magnitude of the current and the shape of the IV curve is nearly identical with 0V or 50V on the gate.

disorder in our system in terms of variation in dot sizes and in lattice imperfections and spacing variations. It may also be accounted for by the fact that Middleton and Wingreen only consider nearest-neighbor hopping in their analysis. As discussed earlier, hopping is not limited to nearest neighbors and long-range interactions are an important component of conduction in semiconductor NC films. Our result is closer to the experimental result obtained by Jaeger et al. [19], who find a power of 2.25 ± 0.1 in arrays of gold nanocrystals and to the results of Rimberg et al. [20], who studied aluminum nanocrystal films and found $\xi = 1.8 \pm 0.16$.

Figure 5-2 shows the IV curves at several gate voltages on a log-log plot. The curves appear linear with a slope of 2.05 on the plot The fit shown in the figure is for the data taken at $V_g = 0V$, but fits were done for all gate voltages shown and $2.0 \leq \xi \leq 2.1$ for each curve.

After annealing, we measured the zero-bias conductance (G) of the film as discussed in Chapter 4. G measurements at gate voltages ranging from -100V to 100V show the conductance to depend strongly on gate voltage at 294K, 150K and 77K (Figure 5-3). However, the dependence is qualitatively much different at 294K than at the lower temperatures. At

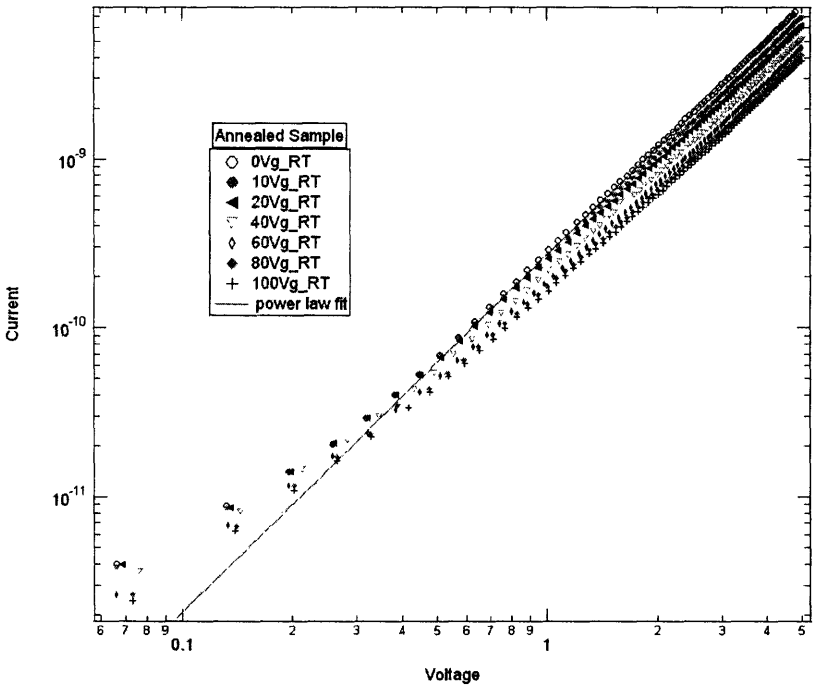

Figure 5-2: **IV curves after annealing.** The curves follow a power law with exponent 2.05.

294K, conductance falls monotonically with increasing gate voltage, implying that holes are the dominant carrier type and that hole concentration increases monotonically from 100V to -100V. At lower temperatures, the curve is U-shaped, with conductance increasing with both positive and negative gate voltages. This implies that both electrons and holes are carriers and that negative gate voltages increase hole concentration while positive gate voltages increase electron concentration.

The change in the shape of the curve with temperature is a little bit confusing. The monotonic decline of conductance with gate voltage at 294K implies either that electrons have very low mobility or a very low injection rate at 294K or that there is an excess of holes at $V_g = 0V$. One possibility is that different localized trap states exist at different temperatures. It is possible that at lower temperatures, the concentrations of hole traps and electron traps are roughly equal, but the holes are able to escape from their traps at between 150K and 294K while the electrons can not escape below 294K. Then the concentration of holes at 294K would be substantially higher than that of electrons, but the concentrations of the two carriers at lower temperatures would be about equal.

To test the validity of equation equation 2.6, the curves at 77K and 150K are fitted with linear fits. This equation is not entirely valid because the first carriers to enter the films will be forced into localized trap states rather than being allowed to enter the conduction band and incrase conductivity, as depicted in Figure 5-4. The localized trap states can be the result of unpassivated polarized sites on the surface of the NC's, potential wells created by the oleic acid, or impurities within the NC's.

Assuming equation 2.6 does apply reasonably well, we can solve for the effective mobility of both electrons and holes in the films. The fits use the equation:

$$G = a * V_g + B \tag{5.2}$$

substituting for V_g from equation 2.9 and observing that $Q/A = m * ne$ for electron injection and $Q/A = -m * pe$ for hole injection, we find

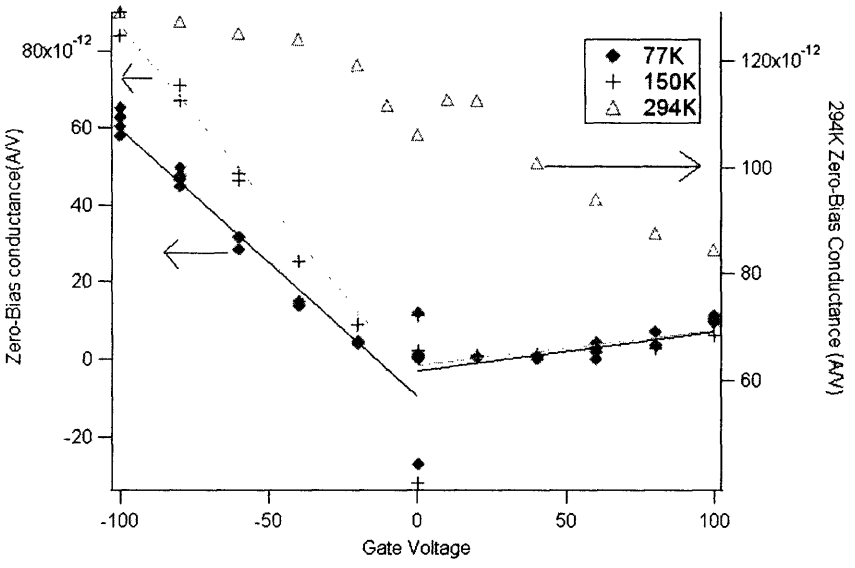

Figure 5-3: **Zero-bias conductance as a function of gate voltage.** This data was taken as follows: at 77K, the sample was measured with V_g = 0V, -20V, -40V, -60V, -80V, -100V, 0V, 20V, 40V, 60V, 80V, 100V, 0V. At 150K, the same sample was measured at the same gate voltages, except the positive gate voltages were measured first stepping upwards from $V_g = 0V$, then the gate was stepped downwards from $V_g = 0V$. However, the 150K measurement was repeated applying negative gate voltages first and the curve was very similar; these data are not shown here. At room temperature, a different sample was measured at the pos. At 294K, the conductance was measured at positive gate voltages on one day and at negative gate voltages on a different day, always stepping from $V_g = 0V$. The 294K data was repeated all in one day on several other samples and the curves were very similar.

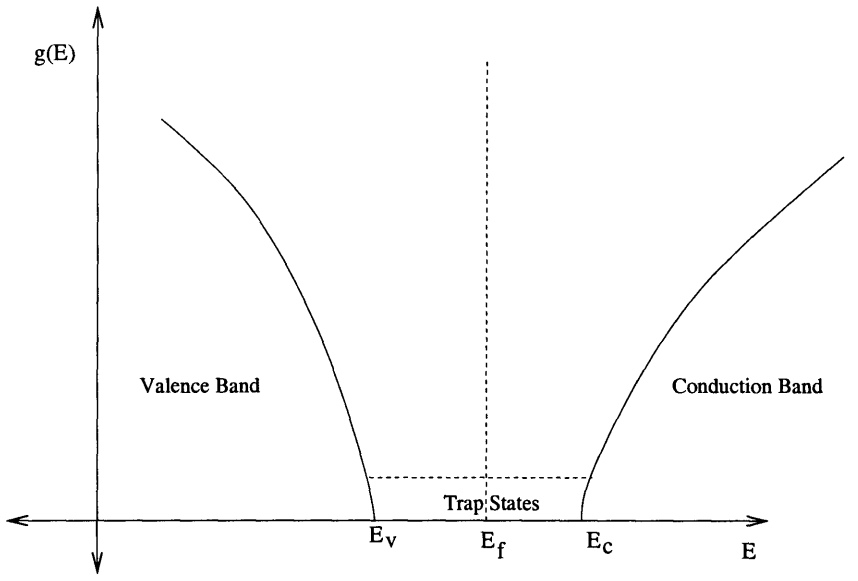

Figure 5-4: **Energy diagram of states available to injected electrons and holes** When charge carriers enter the film at the fermi level (E_f), they must fill up the available trap states before entering the conduction band (electrons) or the valence band (holes).

$$G = a * \frac{d}{\epsilon}(ne) * m + B \tag{5.3}$$

$$G = -a * \frac{d}{\epsilon}(pe) * m + B \tag{5.4}$$

where m is the depth of the film. Conductance (G) and conductivity (σ) are related by

$$\sigma = \frac{GL}{A} \tag{5.5}$$

plugging this into equation 5.3, we find

$$\sigma = \frac{l}{w * m} * a * \frac{d}{\epsilon}(ne) * m + B \tag{5.6}$$

Table 5.1: **Linear fit parameters, and effective mobilities of electrons and holes.**

Temperature	$V_g > 0$	$V_g < 0$	a (A/V^2)	b(A/V)	$\mu_e(cm^2V^{-1}s^{-1})$	μ_h	σ_μ
150K		x	-9.30E-13	-6.49E-12		4.71e-7	2.59e-8
150K	x		1.01E-13	-3.16E-12	5.12e-8		3.69e-8
77K		x	-6.93E-13	-9.59E-12		3.51e-7	1.36e-8
77K	x		8.95E-14	-1.48E-12	4.54e-8		1.57e-8

$$\sigma = \frac{l}{w * m} * (-a) * \frac{d}{\epsilon}(pe) * m + B \tag{5.7}$$

where l is the length of the current path across the gap and w is the width the electrodes along the gap. In our devices, $l = 1\mu m$ and $w = 200\mu m$. Comparing these equations to equation 2.6 and assuming that only holes are injected at positive V_g and only electrons at negative V_g, we see that

$$\mu_e = a * \frac{dl}{w\epsilon} \tag{5.8}$$

$$\mu_p = -a * \frac{dl}{w\epsilon} \tag{5.9}$$

Using the above equation, we calculate μ_e and μ_h based on the fits in Figure 5-3. The results of these calculations, along with the fit parameters, are shown in Table 5.1.

Since not all of the carriers are injected into the film, e and p, the concentrations of carriers, are lower than anticipated. Thus, when we solve for the mobility, we will be using a higher concentration than is actually in the film, so the effective mobility we find will be a lower bound on the actual effective mobility. It is important to note that the term "mobility" in a bulk semiconductor refers to a function of the velocity and mean free path of the charge carrier. In an NC film where conduction occurs by tunneling, neither velocity nor mean free path are meaningful characteristics of charge carriers, so when we find an effective mobility, the quantity does not have the same physical interpretation as it does for more

traditional materials. However, equation 2.6 still has an important physical interpretation, that conductivity should rise in proportion to charge carriers.

Because of the localized trap states present in the films and the fundamental differences in conduction physics between our films and the materials for which equation 2.6 is derived, the above analysis is a substantial simplification of the processes that actually produce V_g-dependence of the conductance. This is apparent in the imperfection of the linear fits to the data in Figure 5-3.

Our results show mobilities that change little between 77K and 150K. Both mobilities do drop slightly as temperature falls, but the difference is smaller than σ_μ. Lower mobility at lower temperature makes sense because there is less thermal energy to enable electrons to tunnel between NC's. At both temperatures, μ_e is substantially smaller than μ_h and μ_e is only about twice as large as its standard deviation, σ_μ. Thus, it is possible that conductance is not actually increasing with positive gate voltages. This would mean either that μ_e is much smaller than μ_h, as calculated, or it could mean that there are many more electron trap states in the film than hole traps. The data indicate the latter case. The minimum of the conductance curve is actually not at zero gate voltage. The curve is essentially flat, and even falling somewhat between $V_g = 0V$ and $V_g = 20V$. This implies that when positive gate voltage is first applied, electrons are pulled into trap states and do not increase conductivity at all until V_g rises above 20V. The mobilites we calculate are much smaller than those in bulk PbSe, as expected. At 300K, μ_e and μ_h are $1000cm^2V^{-1}s^{-1}$. At 77K, $\mu_e = 16500cm^2V^{-1}s^{-1}$ and $\mu_h = 13700cm^2V^{-1}s^{-1}$ [21] for bulk PbSe. Measurements of photocurrent in unannealed PbSe films indicate mobilities on the order of $\sim 10^{-10}cm^2V^{-1}s^{-1}$, much smaller than what we've calculated here. Because it is difficult to estimate the carrier concentration based on photoconductivity measurements, this number may not be very accurate, but it indicates that annealing may increase mobility substantially.

Figure 5-5 shows the magnitude of the current as a function of V_g. What is displayed is the difference between the current at $V_g = 5V$ and the current at $V_g = -5V$. The differential measurement prevents offsets resulting from leakage current from the gate from affecting the

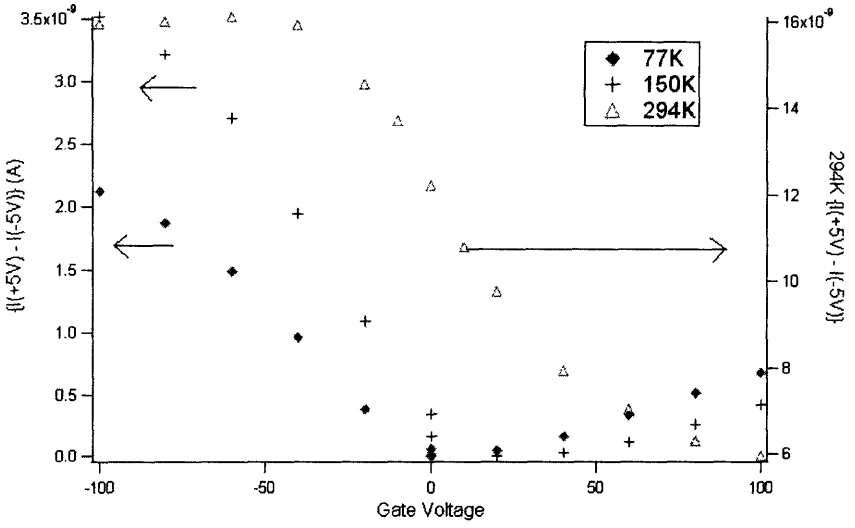

Figure 5-5: **Current as a function of gate voltage.** The current curves follow shapes very similar to the zero-bias conductance. The current shows a much stronger gate voltage dependence than the conductance does at 294K. At 150K and 77K, the behavior has changed very little between $V_{sd} = 0V$ and $V_{sd} = 5V$. This plot is made wwith current data from the same measurements used to make Figure 5-3

data. It is interesting that these curves follow the same general shape as the zero-bias conductance curves and that at 77K and 150K the shapes of the current curves are very similar to the shapes of the conductance curves. Because the current does not vary linearly with time, it is important that V_g dependence does not vary significantly with source-drain bias or current size. If the V_g dependence changed with increasing V_{sd}, the model we are using would be called into question. Adding charge carriers should increase conductance uniformly regardless of applied electric field.

Both the conductance and current measurements show a change in temperature dependence at different gate voltages. At $V_g = -100V$, we see conductance rise by a factor of 2 and current rise by a factor of 8 between 77K and 294K. However, at $V_g = 0V$, we see both current and conductance rise by a factor greater than 100 between 77K and 294K. It is interesting that we can see such weak temperature dependence in the conductance by applying a large negative gate voltage. A simplistic model would predict strong temperature dependence of the conductance regardless of gate voltage due to a greater propensity

for charge carriers to become trapped when less thermal energy is available to them. The conductance does in fact depend very strongly on temperature when there is no gate voltage applied, and this dependence essentially disappears as V_g falls.

Chapter 6

Discussion

6.1 Annealing Data

The increases in conductance while annealing are impressive. Additionally, the apparent onset of V_g dependence after annealing is interesting, but needs to be further investigated before concluding that there is no V_g dependence before annealing. It is possible that very low mobilities before annealing makes charge injection difficult, reducing the ability of the gate to increase conductance.

The potential to further increase conductance by annealing at higher temperatures should be explored. Annealing at 500K has resulted in substantial optical changes in the film. The film turns from irridescent to dull gray colored and shows cracking, especially near the edges and near where gold wire is bonded to the electrodes. What these changes indicate is unclear since no TEM images have been taken after annealing at temperatures above 400K. These films were unmeasurable due to excessive leakage current to the gate. Since it is clear that chemical changes in the film require annealing at temperatures above 410K, more investigation should be done into high temperature annealing. Higher temperatures also offer the potential to reduce the time required for annealing substantially.

6.2 Gate Voltage Data

The strong dependence of conductivity on gate voltage is an exciting result. It indicates that both electrons and holes can be capacitively injected into PbSe films from gold electrodes. Indeed, PbSe is a material that is much more amenable to charge injection than CdSe and it is much easier to observe currents and conductivity changes. This is the first time, to our knowledhge, that gate dependence of dark current has been observed in arrays of colloidal semiconductor nanocrystals and thus this is a very important result.

The change in V_g dependence with temperature warrants subtantial further work. No measurements have yet been made between 150K and 294K, but this temperature regime is clearly interesting and more investigation of the V_g dependence of the conductance in this range may yield information that will give a much better picture of the mechanisms for conductivity changes and how and why they vary with temperature. If the hypothesis presented in Chapter 4, that holes escape from their traps between 150K and 294K, is true, a sharp transition from the kind of behavior we see at 150K and the kind we see at 294K would be expected at the temperature that releases the holes. If the temperature dependence of the behavior instead results from a change in the mobility of holes and electrons with temperature, the transition may be smoother. The lack of temperature dependence in the conductance at $V_g = -100V$ is a surprising and important result.

6.3 Conclusion

PbSe NC arrays offer a lot of promise for exciting and unique electrical transport properties. Because semiconductor NC arrays are a relatively new area of research, there is a lot to learn about how they behave and what they may be used for. Perhaps collective effects will be observed that will open the door to powerful computing applications. Perhaps it will be some entirely different and unexpected property of the films that turns out to change an industry or start a new one. Even if a highly demanded or industry changing application is never found for semiconductor NC's, their ability to model atomic systems and basic

potential wells will inevitably lead to substantially expanded and enhanced understanding of fundamental physical principles.

Bibliography

[1] C.B. Murray, C.R. Kagan, M.G. Bawendi, Annu. Rev. Mater. Sci. **30**, 545-610 (2000)

[2] N.Y. Morgan, C.A. Leatherdale, M. Drndić, M.V. Jarosz, M.A. Kastner, M.G. Bawendi, Phys. Rev. B **66**, 075339 (2002)

[3] C.A. Leatherdale, C.R. Kagan, N.Y. Morgan, S.A. Empedocles, M.A. Kastner, M.G. Bawendi, Phys. Rev. B **62**, 2669 (2000)

[4] H. Du, C. Chen, R. Krishnan, T.D. Krauss, J.M. Harbold, F.W. Wise, M.G. Thomas, J. Silcox, Nano Letters **2**, 1321 (2002)

[5] B.L. Wehrenberg, P. Guyot-Sionnest, J. Am. Chem. Soc. **125**, 7806 (2003)

[6] B.L. Wehrenberg, P. Guyot-Sionnest, J. Phys. Chem. B **106**, 10634 (2002)

[7] W.W. Yu, J.C. Faulkner, B.S. Shih, V. L. Colvin, Chem. Mater. **16**, 3318 (2004)

[8] C.B. Murray, S. Sun, W. Gaschler, H. Doyle, T.A. Betley, C.R. Kagan, IBM J. Res. & Dev. **45**, 47 (2001)

[9] J.S. Steckel, S. Coe-Sullivan, V. Bulović, M.G. Bawendi, Adv Mater. **15**, 1862 (2003)

[10] E. Lifshitz, M. Bashouti, V. Kloper, A. Kigel, M.S. Eisen, S. Berger, Nano Letters **3**, 857 (2003)

[11] S. Bandyobadhyay, V. Roychowdhury, Jpn. J. Appl. Phys. **35**, 3350 (1996)

[12] J.J. Hopfield, Proc. Natl. Acad. Sci. USA **79**, 2554 (1982)

[13] D. Yu, B. L. Wehrenberg, P. Guyot-Sionnest, Phys. Rev. Lett. **92**, 216802 (2004)

[14] A.A. Middleton, N.S. Wingreen, Phys. Rev. Lett. **71**, 3198 (1993)

[15] C.P. Bean, Phys. Rev. Lett. **8**, 250 (1962)

[16] D. Yu, C. Wang, P. Guyot-Sionnest, Science **300**, 1277 (2003)

[17] L.S. Levitov, B. Kozinsky, arXiv:cond-mat/9912484 (1999)

[18] M. Drndić, M.V. Jarosz, N.Y. Morgan, M.A. Kastner, M.G. Bawendi, J. Appl. Phys. **92**, 7498 (2002)

[19] R. Parthasarathy, X.M. Lin, H.M. Jaeger, Phys. Rev. Lett. **87**, 186807 (2001)

[20] A.J. Rimberg, T.R. Ho, J. Clarke, Phys. Rev. Lett. **74**, 4717 (1995)

[21] Y.L. Ravich, B.A. Efimov, L.A. Smirnov, in *Semiconducting Lead Chalcogenides* (Plenum, New York, 1970), Appendix C